Improving Earth's magnetic field measurements by numerical corrections of thermal drifts and man-made disturbances

Michal Janošek[1]*, Mattia Butta[1], Michal Vlk[2] and Tomáš Bayer[2]

[1] Department of Measurement, Faculty of Electrical Engineering, Czech Technical University in Prague, Czech Republic; janosem@fel.cvut.cz
[2] Institute of Geophysics, Czech Academy of Sciences, Prague, Czech Republic; vlk@ig.cas.cz
* Correspondence: janosem@fel.cvut.cz; Tel.: +420-22435-3964

Received: date; Accepted: date; Published: date

Abstract: This contribution deals with challenges encountered in real-world geomagnetic measurements, and is focused on improving the performance of two variometer stations of Kelčany and Polom, which have been recently established in the Czech Republic. It is shown that a carefully designed full-field instrument, despite lacking temperature stabilization, can provide vectorial and scalar data accurate to a few nT, if the raw data were post-processed by compensating for gain temperature coefficients – we show how this can be obtained by a precise calibration and long-term scalar measurements. We also show a method for suppressing nT-level spikes in the data due to nearby car traffic, by utilizing gradiometric measurement for detecting the car occurrences and by employing a linear optimization problem in order to find the parameters of the moving magnetic dipole and compensate for it. In this manner, we were able to reduce the anthropogenous noise due to car traffic while keeping as much original information as possible.

Keywords: variometer; disturbance; Earth's magnetic field

1. Introduction

Vectorial magnetometers which serve for monitoring of Earth's field variations due to diurnal field changes, geomagnetic storms, etc., are standard instruments deployed at geomagnetic observatories and variation stations; they are mostly based on fluxgate sensors [1]. To achieve the best magnetometer (variometer) performance, it will be usually installed in a temperature-stabilized environment, either by the use of an active, magnetically clean heating-system or by selecting a highly temperature-stable location, preferably underground. This approach is of course demanding on the site selection and/or the necessary infrastructure. However, the variometer performance improved recently not only in terms of noise (the current state-of-the art noise limit of fluxgate sensors is about 3-5 pT/√Hz @ 1 Hz) but also in temperature stability [1]-[3]. Also, with the advent of dc-precise 24-bit A/D converters, it is possible to build a „full-field" instrument which can not only monitor the magnetic field variations, but also can provide the vector magnitude (scalar) from the three vector components. To achieve this, precise magnetometer calibrations are needed [4], [5] and the calibration parameters need to be long-term stable. The calculated total field value can be further used for temperature compensations.

An important aspect of real-world deployment of variometers is the anthropogenous noise at the selected site, which is at least in Central European region difficult to obey by placing the instrument in a remote locality - due to extensive urban development, DC-railways, pipelines etc. [6]. Thus, the anthropogenic noise should be estimated and, if better location is not viable, a compensating or at least a detection method should be developed; the latter is the case mainly if the occurring disturbances are on local-scale, i.e. car-traffic - we will show this is the case of one of our localities.

The following results were obtained from magnetometers running at three different localities in the Czech Republic. The reference, low-noise data was obtained from the established INTERMAGNET geomagnetic observatory Budkov (BDV) in Southern Bohemia, which employs passive and active

temperature stabilization. Two variometer stations were recently established – Polom (PLM) in Eastern Bohemia at the Czech-Polish border and Kelčany (KEL) in south Moravia – see Fig. 1. The motivation to have all three stations is clear - first, having data redundancy is important for magnetic field observations, forecasts and data services, moreover from three measurements it would be theoretically possible to suppress the anthropogenous noise which occurs on local-scale - the only correlated information is the Earth's field variation, which is homogeneous enough across the three stations span (100 - 200 km). From Fig. 1 it is evident, that mainly the DC railways (which are far away from BDV observatory) will have a detrimental effect on anthropogenic noise on both variometers running at PLM and KEL. The site of Průhonice (PRU) just at the outskirts of Prague is also shown; it served as a geomagnetic observatory station from 1946 to 1967, when the magnetic observations have been moved to a much quieter location of Budkov.

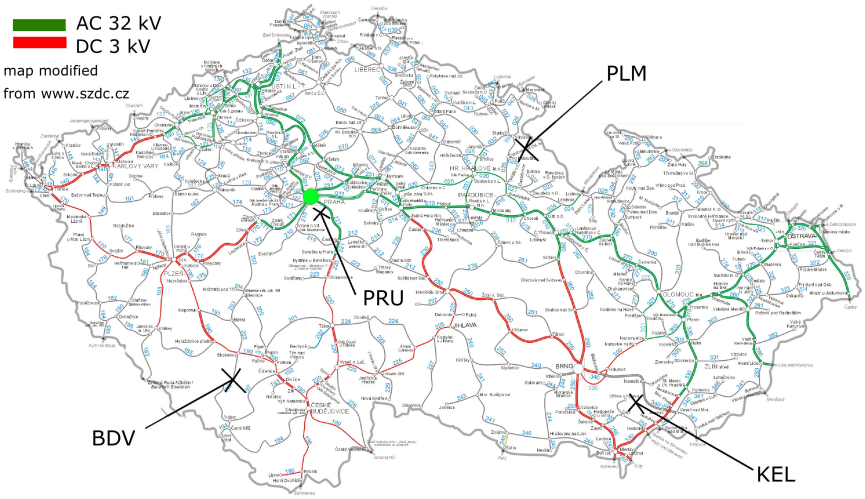

Figure 1. Budkov (BDV), Polom (PLM) and Kelčany (KEL) sites location. Background image is the Czech railway network electrification - green is DC traction, red is AC 50 Hz (modified from [7]). Ex-observatory site Průhonice (PRU) is shown to illustrate moving away from human-made noise.

2. Instrument setup and site limitations of PLM and KEL stations

The station of Polom (PLM) has been in service since late 2016. The site is a property of Czech Army and is being run in collaboration with Institute of Geophysics, CAS, and provides important seismic, meteorological and geodetic data [8]. CTU and IG CAS took the opportunity to install a fluxgate variometer instrument [4] in the already magnetically pre-screened and prepared locality. Because of the recent installation, temperature-stabilized hut is not yet available and therefore the variometer sensor and also electronics are operating at ambient temperatures, although protected from the elements. The site is also equipped with non-magnetic pillars for obtaining „absolute" magnetic measurements, i.e. measurements of local inclination and declination hand-to hand with total field intensity, which are usually obtained using a portable Overhauser magnetometer [9].

The station of Kelčany (KEL) is privately-owned and is being run by the members of Magnetic Laboratory at the Department of Measurement, FEE CTU Prague. The advantage of the site compared to PLM is the underground location of the sensor and electronics (in a dual-purpose wine-cellar), which allows for less than ± 5°C yearly temperature variation. Careful magnetic mapping has been done before installation, the site was cleaned of ferromagnetic objects and a non-magnetic pillar for the instrument was built. The site is running since 2015 and is - advantageously - on roughly the same latitude as the BDV observatory. The data are publicly available [10].

The magnetometers installed both at KEL and PLM stations were manufactured at the CTU using low-noise race-track fluxgate sensors, exhibiting ~20 pT digital noise floor and showing high geometrical and temperature stability. The triaxial sensor head at PLM is moreover made from MACOR machinable ceramics; the head is further fixed on a marble plate [3] - see Fig. 2. Neither KEL nor PLM facilitate a scalar magnetometer, thus the total field data are calculated from the three orthogonal field components.

(a) **(b)**

Figure 2. (a) The triaxial sensor head (1) at PLM station is placed in an unheated hut made of PVC (3) and is surrounded by non-magnetic white bricks to increase the thermal mass (2). The hut is painted with special sun-reflecting paint. **(b)** The sensor at KEL variation station is located 6-m underground.

After initial trials at the PLM station, where the ambient temperature can change from -20°C to +40°C, we decided to orient the sensor to the "UVZ" orientation [11]. This means that the two horizontal axes are oriented ± 45° from local meridian - in this manner, both horizontal axes are measuring roughly the same magnetic field (about 15,000 nT at our location). The NEZ or HDZ components are computed numerically [9], so the offset drifts and mechanical instability in azimuth are of less significance than if measuring the E or D component directly. Also the compensating current in all axes is large enough (few mA) not to be influenced by cable leakage currents. The UVZ orientation is also beneficial for obtaining a simple thermal drift model as shown later.

A comparison of anthropogenous noise observed at BDV, KEL and PLM stations is shown in time-domain in Fig. 3, where the calculated total field from both KEL and PLM vectorial readings is compared to total field measurements at BDV observatory provided by Overhauser magnetometer.

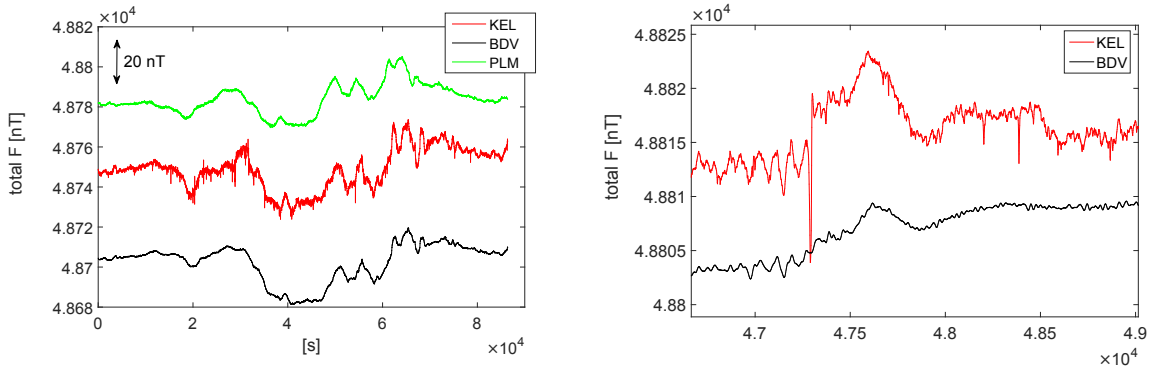

(a) **(b)**

Figure 3. (a) 1-day total field variation recorded at Budkov (BDV - black), Polom (PLM - green) and Kelčany (KEL - red). It is clearly seen that lowest-noise occurs at BDV, followed by PLM showing distant anthropogenic noise and KEL exhibiting large, fast spikes, most probably from car traffic. Offsets are caused by different site geology and instrument calibrations. **(b)** KEL and BDV in detail.

The anthropogenous noise at both PLM and KEL is larger than at the BDV observatory (about 0.2 nT peak-peak), however at KEL also isolated peaks occur with an amplitude up to several tens of nT p-p, which have been later traced down to be caused by nearby car-traffic, as is further shown in section 2.2.1.

Figure 4 further shows aligned spectrograms from three days of 1-second data obtained at all three sites (21-23/7/2017). At PLM the clean nights are alternated with noisy daytime periods due to the ~ 40 km distant DC railway and light urban rail. Although the noise at BDV station is very low, the used instrument (DMI

Fluxgate variometer) has large intrinsic noise, so actually during the quiet night periods (with almost no electric train traffic) the PLM data are less noisy due to the used variometer. The KEL data on the other hand suffer from increased anthropogenic noise even during the night, since the sensor is located in a residential location - the broadband daytime noise is another 10 dB above PLM. Another 10-20 dB noise increase in short bursts has been traced down as local car traffic.

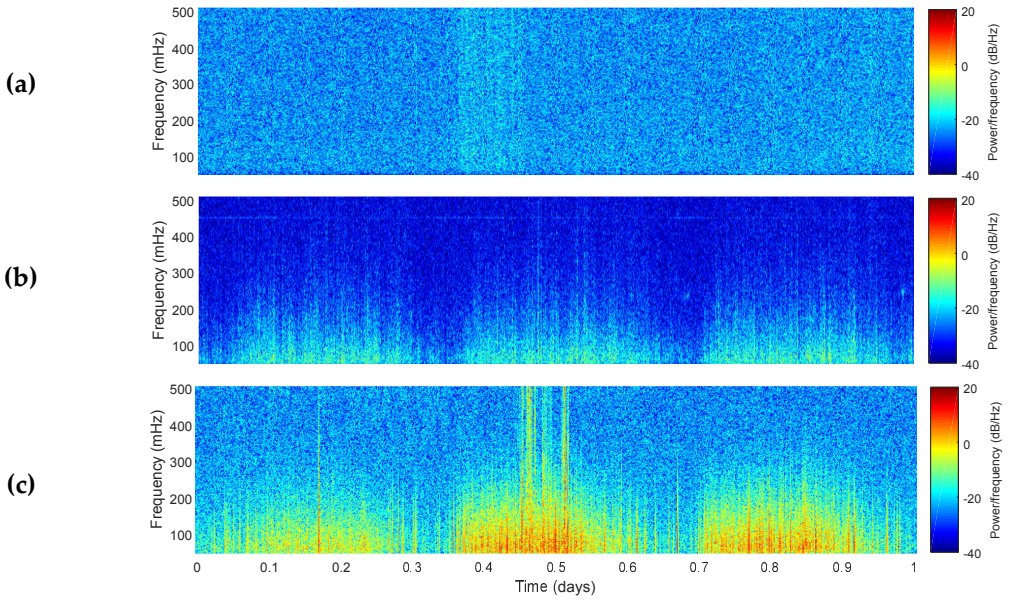

Figure 4. The power spectral density of 1-Hz magnetic data (vertical component, diurnal variation removed) at BDV **(a)**, PLM **(b)** and KEL **(c)** shows that the anthropogenic repeats on a daily-scale, with quiet night periods and noise bursts in daytime.

2.1. Car traffic and magnetic noise

To confirm the origin of the excess-noise at KEL site, the passing cars (the local street is about 25-m away from the sensor location) have been observed by a web-camera and by a cell-phone video recording, respectively and compared to magnetic data - a sketch displaying the actual setup at KEL site is shown in Fig. 5.

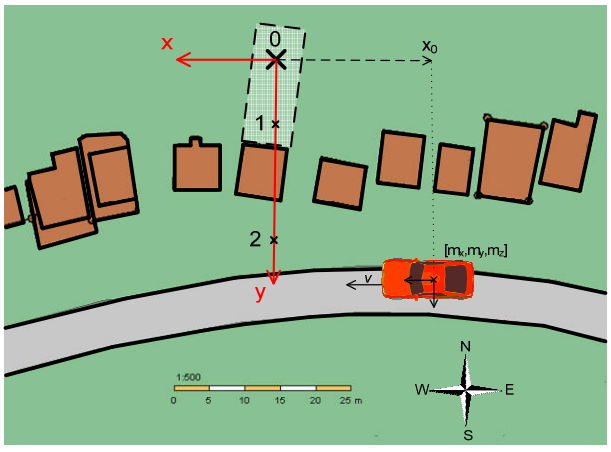

Figure 5. Sketch of the situation at KEL station: the variometer sensor (0) is located approximately 25-m from a frequent local street, which is running roughly in E-W (x) direction. The car occurrences were measured at the central line in the N-S direction, thus in the magnetic sensor "y" coordinate. Positions 1 and 2 show the locations of the second sensor and gradiometer, respectively.

To be able to detect, mark and possibly remove the passing car's magnetic signature, an axial (dB_y/dy) fluxgate gradiometer has been created in N-S direction by placing a second sensor coaxial to the variometer head. This second sensor has been placed approx. 5 m away from the variometer (position 1), closer to the street; later also a short-baseline gradiometer was placed at position 2. The peaks obtained from the axial gradient data correspond with the peaks of the variometer data; however the gradiometer noise floor is still high for detecting spikes less than about 5 nT p-p.

On Fig. 6 the vehicle occurrences have been drawn into the magnetic field recorded. Axial gradient (in N-S direction) and magnetic field (N-S component) are shown - the recorded spikes are in the order of tens nT p-p (even larger for vans/ busses), we show that there is a clear correlation of the spikes and car traffic.

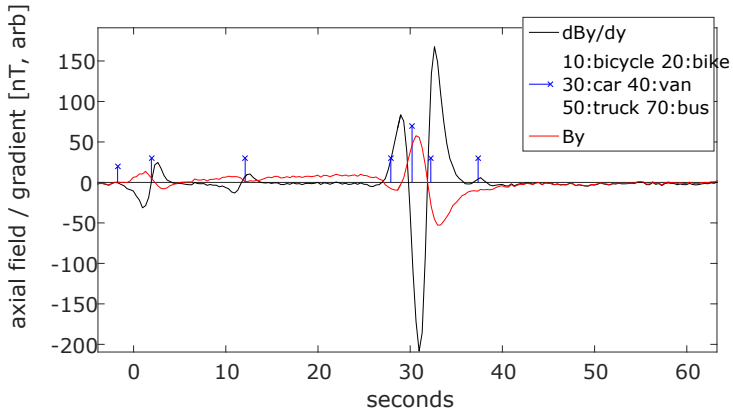

Figure 6 The vehicle occurrences and magnetic field / axial gradient in N-S direction. The strongest disturbance occurs for a bus running in the closer lane - about 110 nT p-p.

3. Methods of improving the real-world performance at KEL and PLM stations

At KEL and PLM sites, we are experiencing two difficulties: temperature drifts due to seasonal and diurnal changes of the ambient temperature (PLM) and large noise due to car occurrences (KEL). It should be noted that the car-induced spikes cannot be simply filtered out with a low-pass filter, since the peaks in the individual axes are not bipolar, thus any low-pass filtration would introduce artefacts in the measured data. Moreover, for a strong magnetic source (e.g. a bus-coach), the disturbance occurs even for 20 seconds.

3.1. Correcting for temperature drifts (PLM)

It is obvious that if the temperature coefficients of the sensor are known (i.e. offset and gain temperature coefficient), one could recalculate and obtain drift-free data. However, the temperature drift in a fluxgate magnetometer (assuming that the electronic is drift-free) is caused by multiple effects [12], e.g. by temperature of the excitation tank capacitor, by dimensional expansion of the feedback/pick-up coil or due to the expansion of the triaxial holder material and its base. Moreover it is difficult to calibrate the whole setup as the sensor and its base are quite bulky. As we have selected the UVZ orientation of the sensor, the ~20-30 ppm·K^{-1} sensitivity drifts dominate in all axes, simplifying further modeling of thermal response[1]. The predicted sensitivity drift is 0.4 nT·K^{-1} for each horizontal axis and 1.1 nT·K^{-1} for the vertical axis, respectively. Utilizing a "full-field" variometer, thus measuring in a feedback loop all the three vector components of the magnetic field at once, allows us for calculation of the total magnetic field (the scalar vector magnitude). Both variometers at PLM and KEL have been calibrated with the "scalar method" [4] for

[1] With NEZ orientation, the E axis drift would be dominated by offset drift which is a combination of electronic and sensor drifts; however the electronics and sensor head are in our case at different positions and temperatures and exhibit different thermal mass. With HDZ orientation, the D component (~ 2000 nT) would be influenced both by offset and gain drifts. In both NEZ and HDZ cases, also mechanical directional instability would have to be modeled.

their offsets, gains and orthogonalities, so the only difference to a drift-free scalar measurement from an Overhauser magnetometer are then the magnetometer drifts itself.

We did this for the PLM variometer by comparing the Overhauser readings obtained at BDV observatory to the calculated total field from PLM - in this case we assume that on the local scale, the measurements at the two localities, which do not exhibit geologic anomalies, will differ only by a stable offset $\boldsymbol{B}_{\mathrm{Off}}$. This was also verified during multiple on-site measurements with an Overhauser magnetometer at different times and temperatures (we could not yet perform a long-term scalar measurement due to the lacking infrastructure).

To find the actual variometer drifts in all three axes, we have utilized a least-squares fitting method, which generally minimizes the difference B_{Diff} between the scalar reading B_{BDV} at the BDV observatory and the calculated scalar value at PLM from the three individual components B_1, B_2, B_3. Thus we try to minimize B_{Diff} from a large set of following equations:

$$B_{BDV} - \sqrt{\left[(1+\alpha\theta)\cdot B_{1PLM}\right]^2 + \left[(1+\beta\theta)\cdot B_{2PLM}\right]^2 + \left[(1+\gamma\theta)\cdot B_{3PLM}\right]^2} - B_{Off} = B_{Diff}\,. \qquad (1)$$

The solution of Eq. 1 was found with a constrained *fminsearch* function in MATLAB R2015 [13], and the offset B_{off} agreed well with the one obtained from onsite Overhauser measurements. After correcting on the obtained drift constants α, β and γ [T·K^{-1}], we were able to largely suppress the temperature drifts in all three axes. The dataset we have used was from February 2018, which allowed for large temperature span between +17 °C and -12 °C - see Figure 7.

We could improve the results even further by introducing a lag of 800 s which was experimentally obtained by calculating the cross-correlation between the total field differences and temperature - this delay is believed to originate from the fact, that the temperature measurements occur at the MACOR cube where the sensors are located, but significant part of the drifts can be caused by the excitation capacitor temperature coefficient [14] - the capacitor is heated only by radiation, since it is thermally connected to the MACOR cube only by its thin leads. After introducing this delay, the calculated values were following:

α =1.11 β= -2.5 γ=0.37 [nT· K^{-1}] and B_{off} = 417 [nT]

The value of α roughly corresponds to the 30 ppm predicted drift (vertical axis measuring approx. 44 000 nT). Also the γ value corresponds to expected value for a horizontal sensor. However the obtained value of β is unexpected, since both horizontal sensors should exhibit the same values or at least the same order of magnitude. We cannot currently offer other explanation than a faulty sensor deployed at this position.

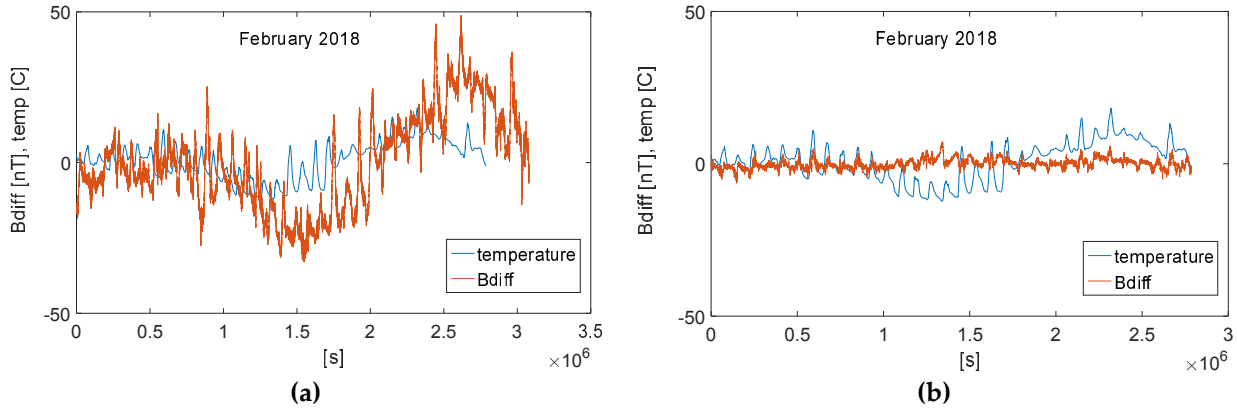

Figure 7 (a) Without temperature compensation, the difference between PLM and BDV scalar values (B_{Diff}) is temperature-dependent and varying between -30 nT to +50 nT. **(b)** After temperature compensation, the B_{Diff} decreased one order of magnitude (to about 5 nT maximum during the freezing temperatures). The data were obtained in February to with -12 to +17°C temperature swing.

After rotating the temperature-compensated PLM vector readings with a 3×3 matrix, which reorients the sensor at PLM to the orientation at BDV, we were able to show that the temperature compensation was successful also in the individual components - see Figure 8.

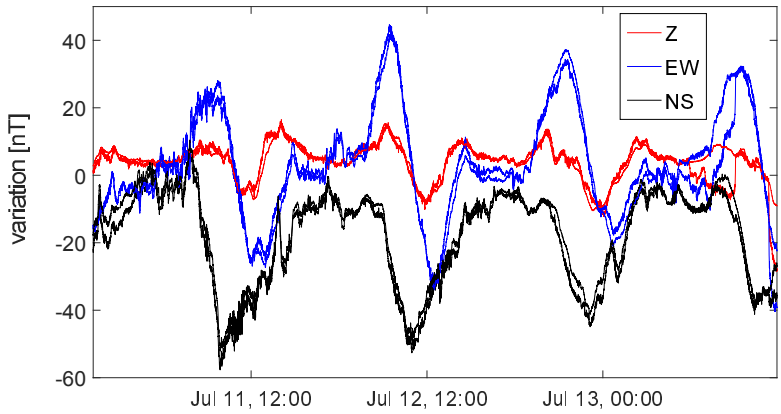

Figure 8. Comparison of aligned BDV and PLM magnetometer readings (the mean is removed to show only Earth's field variations) during three days in July 2017. The difference is well below 5 nT during the observed 14 °C ambient temperature swing. The divergences near the dataset end were caused by false temperature readings.

3.2 Suppressing the car-induced disturbances (KEL)

As we have shown in paragraph 2.1, there is a clear correlation of the disturbances occurring at KEL and the car traffic. Thus we decided to create a simple model, assuming following simplifications:

1. The car at the ~ 25 m+ distance can be well modeled as a single magnetic dipole.
2. We neglect the road curvature and assume it in E-W direction (x-axis).
3. The magnetic moment magnitude and orientation are stable during the car passage, since it keeps its orientation to the Earth's magnetic field.
4. The occurrence of the maximum axial gradient in the y-axis, which occurs when the car radial distance to the sensor is smalles, defines the symmetry point of the car movement,.
5. The maximum axial gradient in the y-axis (N-S component) occurs defines symmetry of the car movement.
6. The car does not change its speed significantly.
7. In 10 seconds, the car is distant enough not to give any significant (> 0.1 nT) disturbance.
8. During the ~20s car passage, the Earth's magnetic field changes only linearly.
9. The occurrences of cars in both lanes are not frequent.

Thus when fulfilling the above assumptions, we can write for the vectors of observed field $\boldsymbol{B}_{Obs} = [B_x, B_y, B_z]$ and vector of car disturbance field $\boldsymbol{B}_{car} = [B_{cx}, B_{cy}, B_{cz}]$ utilizing the well-known equation for magnetic field of a magnetic dipole with magnetic moment $\boldsymbol{m}$ $[m_x, m_y, m_z]$ position vector $\boldsymbol{r}$ $[r_x, r_y, r_z]$ and an (orthogonal) rotation matrix $\boldsymbol{R}$:

$$\vec{B}_{Obs} = \vec{B}_{Earth} + \vec{B}_{Car} = \vec{B}_{Earth} + R\frac{\mu_0}{4\pi}\left[\frac{3\vec{r}\left(\vec{m}\cdot\vec{r}\right)}{r^5} - \frac{\vec{m}}{r^3}\right], \tag{2}$$

where the position vector size (radial distance) r is calculated as

$$r = \sqrt{r_x^{\,2} + r_y^2 + r_z^2}\ . \tag{3}$$

The position vector coordinates of equations 2 and 3 are aligned with the magnetic moment coordinates of the dipolar source (hence the need for rotational matrix $\boldsymbol{R}$ to align with the $\boldsymbol{B}_{Obs}$ coordinates). However we

are not interested in the real orientation of the magnetic moment vector in this case, so there is no need to calculate for $\boldsymbol{R}$, which would further complicate the problem.

To find the "true, disturbance-free" $\boldsymbol{B}_{\text{Earth}}$ of Eq. 2, we have implemented a least-squares fitting-based algorithm, which relies on reading from a gradiometer placed close to the street, allowing for detection of the passing cars through the "point of symmetry". In other words we are trying to fit the magnetic field $\boldsymbol{B}_{\text{obs}}$ at every sampling point using the Equation 2. To achieve this, we implement a set of equations which describe the magnetic field during the short disturbance, which occurs due to the moving magnetic moment. The dataset for the optimization is centered at the gradient peak and is usually 10 + 10 seconds long (Fig 4). Since we assume a simple trajectory as of Figure 4, we are trying to find position components x and y, whereas the only changing is the x, since y is constant and z equals zero in our case. Due to the constant sampling time, we can express x as a linear function of time t and vehicle speed v, both of which we assume constant. Since the sensor at KEL is sampling at 206.5 samples·s^{-1}, there are enough equations during the car passage, even after FIR filtering of the data (to remove 50-Hz mains disturbances) and smoothing. The optimization result of Eq. 2 is then the "true" Earth's field vector $\boldsymbol{B}_{\text{Earth}}$, the magnetic moment vector $\boldsymbol{m}$, the car speed $\boldsymbol{v}$, the initial position x_0 and the constant y distance together with the time-derivative of the Earth's magnetic field during the fitting period.

The optimization is started only when the G_{yy} gradient amplitude in the observed interval crosses a preset threshold in order to run only for disturbances significantly larger than overall system noise. In our case, the threshold has been set to 2 nT·m^{-1}. The algorithm also contains bounds and tests to compensate only using the expected values (car speed ~ 5-20 m·s^{-1}, y between 20 and 30 meters, fitted |m| below 600 A·m^2). For details of the algorithm and used functions, see the Appendix A.

3.2.1 Webcam-trial – magnetic moment statistics

We applied the compensating algorithm on the dataset from the verification video-trial (see Chapter 2.1) in order check the feasibility of our model. In the 50-minutes dataset, we had ~ 270 car passages: 2 bus-coaches, 4 vans, 17 motorbikes and the rest were passenger cars (see Fig. 6 for the induced disturbances), they were evenly distributed in the close and far lane (130 vs. 133 occurrences). The resulting "typical" magnetic moment for passenger cars and busses was found as 250 ± 50 A·m^2 and 520 ± 50 A·m^2, respectively (the compensating algorithm did not start for the motorbikes due to the gradient threshold). In Fig. 9, we show statistics of the individual magnetic moment components (only passenger cars shown), from which it is evident that the largest component is the vertical one which tends to be oriented along the magnetic flux lines, i.e. the m_z component does not change its sign depending on car trajectory orientation.

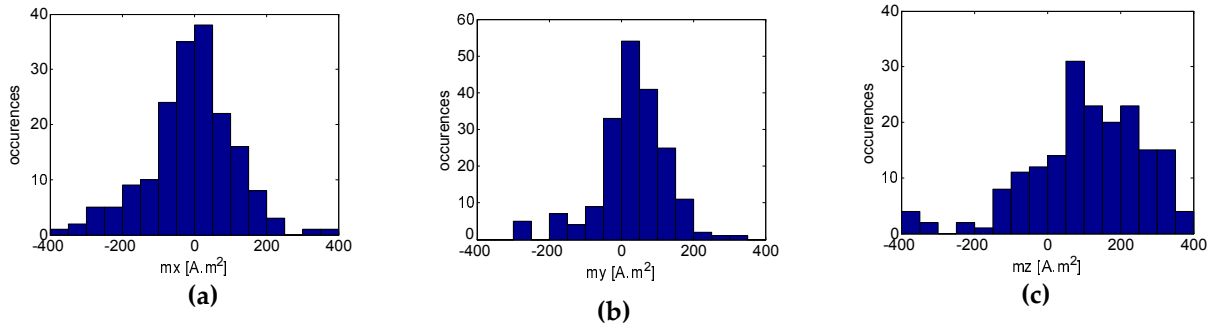

Figure 9 Histogram of magnetic moment components – m_x (**a**), m_y (**b**) and m_z (**c**). The vertical m_z component is statistically larger and unipolar, i.e. it does not change its sign depending on car trajectory orientation

3.2.2 Compensating the disturbances

An example result for compensating a single car disturbance is shown in Fig. 10 - the original data, the fitted dipole from moving car and the data after disturbance compensation are shown for x, y and z field components. The noise clearly decreased in the cleaned-up dataset - see Fig. 11 for a close-up of time-domain and Fig. 12 for two spectrograms of 14-hour data.

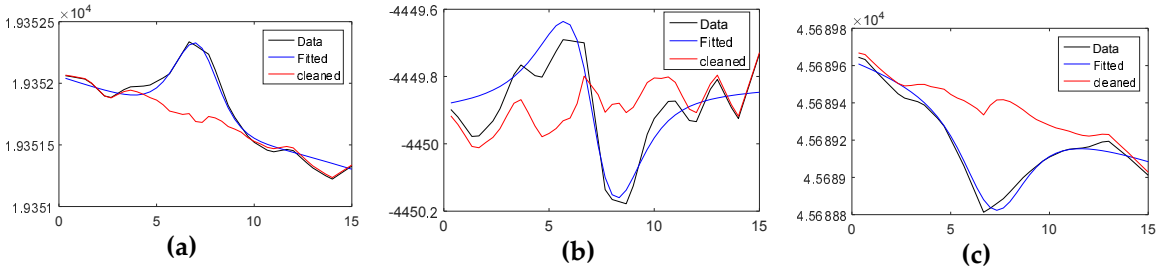

Figure 10 The original data (black), the fitted curve (blue) and the resulting cleaned-up data (red) for the NS-y **(a)**, EW-x **(b)** and vertical-z component **(c)** of the magnetic field, respectively. The car passage occurs at t = 7.5 s. Fitted values were: x_0 = 56 m, v =-7.8 m·s^{-1}, y=19.8m, $\boldsymbol{m}$ = [7, 23.6, 43.5] A·m^2

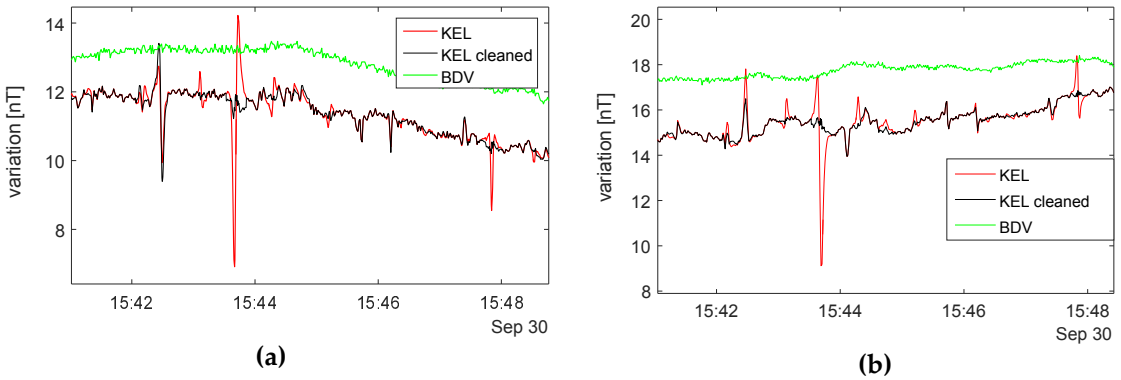

Figure 11 The original (red) and cleaned (black) KEL data compared to the aligned BDV data (5 minutes shown). **(a)** NS-y component, **(b)** EW-x component. The 15:42 (left) peak is not being well compensated, since it occurred when two cars were passing in adjacent lanes and our model fails to find the correct solution. The small uncompensated peaks (about 15:46) did not fit the gradient threshold and/or result tests (see text).

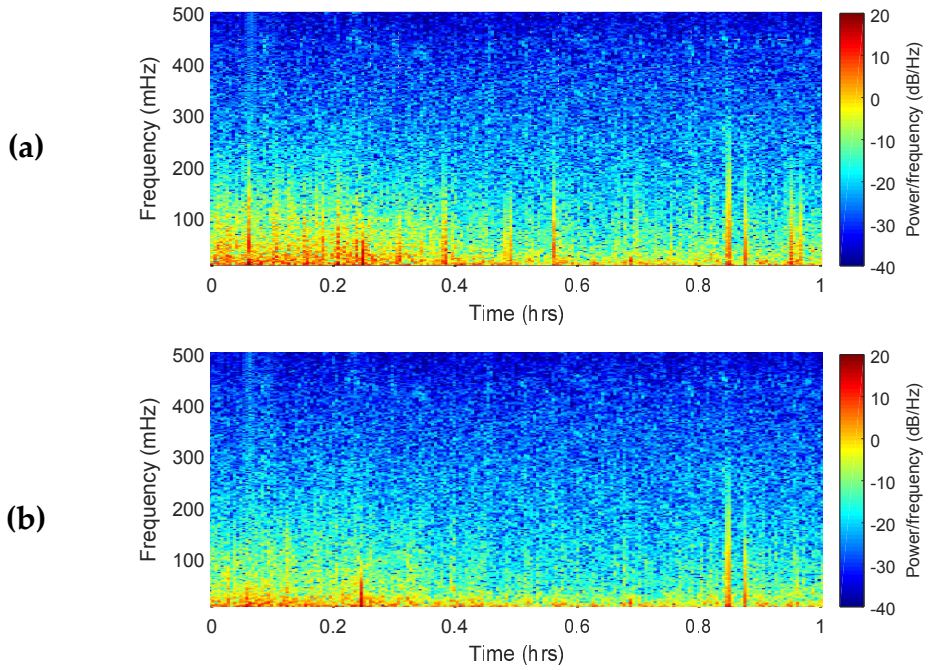

Figure 12 Spectrograms of 14 hours of KEL data (NS - y) - original data with car disturbances **(a)** and after disturbances compensation **(b)**.

4. Conclusion

We show an approach how to deal with 1. unstabilized ambient temperature and 2. man-made disturbances occurring at two variometric stations. Whereas the first problem is usually solved by temperature stabilization – active or passive [15], our approach shows that a "moderate" performance can be achieved even at ambient temperatures. Although the presented method seems straightforward, we are not aware of other ambient-temperature magnetic field stations utilizing such long-term calibration and compensation. The overall maximum residual drift of 5-nT p-p during 30°C temperature swing was achieved, which is even in accordance with INTERMAGNET standards, where the instrument should keep 0.25 $nT \cdot C^{-1}$ for vectorial readings, but it still does not fulfill the required 1nT accuracy for scalar values. However for our purposes this approach brings fast and reliable results as we can really choose the ambient-run site at PLM as redundant source of magnetic data. The steps and results shown here can be beneficial to many "repeat" stations, which usually run at ambient temperatures and which are supplementing the magnetic observatories. Even better results can then be expected if the sensor is i.e. buried at 1-2 meters to avoid such large temperature fluctuations, and of course, when utilizing at least a moderate temperature stabilization (± 2°C), the residual drifts after fitting would be one order of magnitude less than those presented.

As for the second problem, fitting and cleaning of a 14-hours 1-second dataset took less than 60 seconds on a Core-i7 PC using MATLAB R2015, so *off-line* post-processing of daily data could be viable even in embedded systems running Linux and using Python fitting libraries. The fitting speed and accuracy can be improved by having an apriori knowledge of the target y-distance (i.e. knowing the lane) and / or the car speed. For achieving this, distance calculation from axial gradiometer reading [16] or speed measurement with magnetic sensor [18] could be used. Also, improved detection of the passing cars can be facilitated with a short-baseline gradiometer placed as close to the street as possible, which also results in better approximation of the gradient by the calculated field difference. As for the problem with two cars passing in adjacent lanes, it could be possibly solved by employing a second order model with two car trajectories and vector summation of the magnetic signature; for detection of this situation could symmetrically deploy two short-baseline along the street and observe their output in time.

We again emphasize, that this method, when compared to the usual ways - disregarding or interpolating the data, heavy low-pass filtering [9, 19]- allows not only to keep the true DC value, but also does not destroy the "high frequency" component originating from various physical phenomena (field oscillations, solar storm onsets, etc.).

Author Contributions: Conceptualization, Investigation, Software, Methodology, Data curation and Visualization was provided by M.J.; Writing was performed by M.J., M.V. and T.B., Resources and Data collection were provided by M.B., M.J., M.V., and T.B.

Funding: This research received no external funding.

Acknowledgments: We would like to thank to the Military Geographic and Hydrometeorologic Office of the Czech Army for the possibility to work and acquire data at the Meteorologic and Seismic station Polom, including complimentary accommodation; personally to Jaroslav Pokorný for his logistic and technical support during on-site measurements.

Conflicts of Interest: The authors declare no conflict of interest.

Data Availability Statement: The geomagnetic data used to support the findings of this study are available from the corresponding author upon request.

Appendix A

The basic MATLAB function utilized in the optimization problem for car-induced disturbances cancelling is shown in this appendix. The *field-fit* function enters the least-squares curve-fitting algorithm *lsqcurvefit* of the Optimization Toolbox (MATLAB 2015) with a guess of the values and lower and upper bounds; where *xdata* is the time vector and B_{obs} is the vector of observed magnetic field. The function *dip2B* to calculate the field from a point-like, dipolar source follows the dipolar term in Equation 2; an example implementation can be accessed e.g. in [20].

```
function F = field-fit(x,t)
      x0=x(1);  % initial x-distance [m]
      v=x(2);   % car speed [m/s]
      y=x(3);   % y-distance [m]
      m1=x(4);  % magnetic moment components [A.m2]
      m2=x(5);  %
      m3=x(6);  %
      Bx=x(7);  % Earth's field components [nT]
      By=x(8);  %
      Bz=x(9);  %
      dBdtX=x(10); % Earth's field variation (linear) during the disturbance
      dBdtY=x(11); %
      dBdtZ=x(12);%
   [bbx,bby,bbz] = dip2B(x0+t*v,y,0,[m1,m2,m3]);   %% calculating the disturbing field by
                                                                %% moving dipole along
x-coord.
      F(:,1) = Bx + bbx +dBdtX*t;
      F(:,2) = By + bby +dBdtY*t;
      F(:,3) = Bz + bbz +dBdtZ*t;
 end
      x=lsqcurvefit(@field-fit, guess, xdata, Bobs, lb, ub)
```

References

1. Pedersen, L.W.; Merenyi, L. The FGE Magnetometer and the Intermagnet 1 Second Standard. *J. Ind. Geophys. Union* **2016**; 2, 30-36.
2. Marusenkov, A. Possibilities of further improvement of 1 s fluxgate variometers. *Geosci. Instrum. Method. Data Syst.* **2017**; 6, 301-309, DOI 10.5194/gi-6-301-2017
3. Janošek, M.; Petrucha, V.; Vlk, M. Low-noise magnetic observatory variometer with race-track sensors. *IOP Conf. Ser. Mater. Sci. Eng*. **2016**; 108, 012026. DOI 10.1088/1757-899X/108/1/012026
4. Petrucha, V.; Kaspar, P.; Ripka, P.; Merayo, J. M. Automated system for the calibration of magnetometers. *J Appl Phys* **2009**; 105 (7), 07E704, DOI 10.1063/1.3062961.
5. Olsen, N. et al. Calibration of the Ørsted vector magnetometer. *Earth, planets and space* **2003**; 55(1), 11-18.
6. Kompein, N.; Pleschberger, R.; Egli, R.; Leichter, B.; Leonhardt, R. A comparison between Conrad Observatory and the old Wien Cobenzl observatory: Insights into anthropogenic ground currents. In Proceedings of XVII IAGA Workshop on Geomagnetic Observatory Instruments, Data acquisition and Processing, Dourbes, Belgium, 4 September - 10 September 2016.
7. SŽDC - Operation of infrastructure. Available online: http://provoz.szdc.cz/PORTAL/ViewArticle.aspx? oid=594598 (Accessed on 13.6.2018)
8. Laža, L. Four Decades of the Polom Station, *Vojenský geografický obzor* **2014**; 2014, 2, pp. 4-33. In Czech. Available online: http://www.vgo.army.cz/archiv-cisel (Accessed on 13.6.2018)
9. Jankowski, J.; Sucksdorff, C. Guide for magnetic measurements and observatory practice. Boulder: International Association of Geomagnetism and Aeronomy 1996; p. 86. Available online: http://www.iaga-aiga.org/data/uploads/pdf/guides/iaga-guide-observatories.pdf (Accessed on 13.6.2018)

10. Geomagnetic observatory of Kelčany. Available online: https://maglab.fel.cvut.cz/geomagnetic (Accessed on 13.6.2018)
11. Schultz, G. Geomagnetic results Wingst, 2001 - Yearbook No. 47. In: Linthe, H.J. ed: Yearbook Magnetic Results 2001, 2002, 2003; GfZ Potsdam 2007, ISSN 1614-5801 , p. 59
12. Nishio, Y.; Tohyama, F.; Onishi, N. The sensor temperature characteristics of a fluxgate magnetometer by a wide-range temperature test for a Mercury exploration satellite. *Meas Sci Technol* **2007**; 18(8), pp. 2721-2730.
13. D'Errico, J. Bound constrained optimization using fminsearch. In: Math Works - File Exchange. Available online: https://www.mathworks.com/matlabcentral/fileexchange/8277-fminsearchbnd--fminsearchcon (Accessed on 13/6/2018)
14. Cerman, A.; Merayo, J. M.; Brauer, P.; Primdahl, F. Self-compensating excitation of fluxgate sensors for space magnetometers. In: IEEE Instrumentation and Measurement Technology Conference Proceedings, 2008, pp. 2059-2064.
15. Korte, M.; Mandea, M.; Linthe, H. J.; Hemshorn, A.; Kotzé, P.; Ricaldi, E. New geomagnetic field Observations in the South Atlantic Anomaly region. *Annals of Geophysics* **2009;** *52*(1), pp. 65-81.
16. Janošek, M.; Platil, A; Vyhnánek, J. Simple estimation of dipole source z-distance with compact magnetic gradiometer. *IOP Conf. Ser. Mater. Sci. Eng* **2016**; 108(1), 012025, DOI 10.1088/1757-899X/108/1/012025.
17. St-Louis, B. J.; Sauter, E. A.; Coles, R. L. INTERMAGNET Technical Reference Manual, version 4.6, INTERMAGNET 2012. Available online: http://www.intermagnet.org/publications/intermag_4-6.pdf (Accessed on 13.6.2018)
18. Markevicius, V., Navikas, D., Idzkowski, A., Valinevicius, A., Zilys, M., & Andriukaitis, D. Vehicle speed and length estimation using data from two anisotropic magneto-resistive (AMR) sensors. *Sensors*, **2017**; *17*(8), p. 1778.
19. Curto, J. J.; Marsal, S.; Torta, J. M.; Sanclement, E. Removing spikes from magnetic disturbances caused by trains at Ebro Observatory. In: Proceedings of XIII IAGA Workshop on Geomagnetic Observatory Instruments, Data Acquisition and Processing, 2009. US Geological Survey Open File Report 1226, pp. 60-66.
20. University of British Columbia. Potential Fields in Earth and Planetary Sciences. Available online: https://www.eoas.ubc.ca/~malasad/EOSC450 (Accessed on 13.6.2018).